Preprint
UCRL-PROC-201252

Externally Dispersed Interferometry for Resolution Boosting and Doppler Velocimetry

D. J. Erskine

This article was submitted to
2nd Science with SALT Workshop, Capetown, S. Africa, Oct. 29-31, 2003

December 4, 2003

2nd Science With SALT Workshop, Capetown, S.Africa
*ASP Conference Series, Vol. **VOLUME***, 2003*
ed. D. Buckley

Externally Dispersed Interferometry for Resolution Boosting and Doppler Velocimetry

David J. Erskine

Lawrence Livermore Nat. Lab., 7000 East Ave, Livermore, CA 94550

Abstract. Externally dispersed interferometry (EDI) is a rapidly advancing technique for wide bandwidth spectroscopy and radial velocimetry. By placing a small angle-independent interferometer near the slit of an existing spectrograph system, periodic fiducials are embedded on the recorded spectrum. The multiplication of the stellar spectrum times the sinusoidal fiducial net creates a moiré pattern, which manifests high detailed spectral information heterodyned down to low spatial frequencies. The latter can more accurately survive the blurring, distortions and CCD Nyquist limitations of the spectrograph. Hence lower resolution spectrographs can be used to perform high resolution spectroscopy and radial velocimetry (under a Doppler shift the entire moiré pattern shifts in phase). A demonstration of $\sim 2\times$ resolution boosting (100,000 from 50,000) on the Lick Obs. echelle spectrograph is shown. Preliminary data indicating $\sim 8\times$ resolution boost (170,000 from 20,000) using multiple delays has been taken on a linear grating spectrograph.

1. Introduction

An externally dispersed interferometer (EDI) is the series combination of a angle-independent Michelson interferometer (Hilliard & Shepherd 1966) with a grating spectrograph outside the cavity of the interferometer (Fig. 1). The interferometer has a nonzero delay or optical path length difference, typically 1 to 3 cm, that creates a sinusoidal frequency dependence to its transmission. Inclusion of the interferometer into the light beam, like a filter, embeds (multiplies) a comb of very periodic sinusoidal fiducials on the input stellar spectrum, over the entire bandwidth of the spectrograph. The EDI therefore has a simultaneous bandwidth advantage over internally dispersed interferometers (Holographic Heterodyning Spectrograph, Spatial Heterodyning Spectrograph) (Douglas 1997; Harlander, Reynold, & Roesler 1992) which have a limited bandwidth due to their rapid change in fringe periodicity vs wavelength.

Through a heterodyning effect between the fiducials and stellar spectrum, high resolution spectral information is encoded as broad moiré patterns which better survive slit blurring and resist instrumental drifts, allowing use of lower resolution spectrographs. Data reduction arithmetically separates fringing from ordinary spectra, and the fringing component is processed in different ways depending on the application.

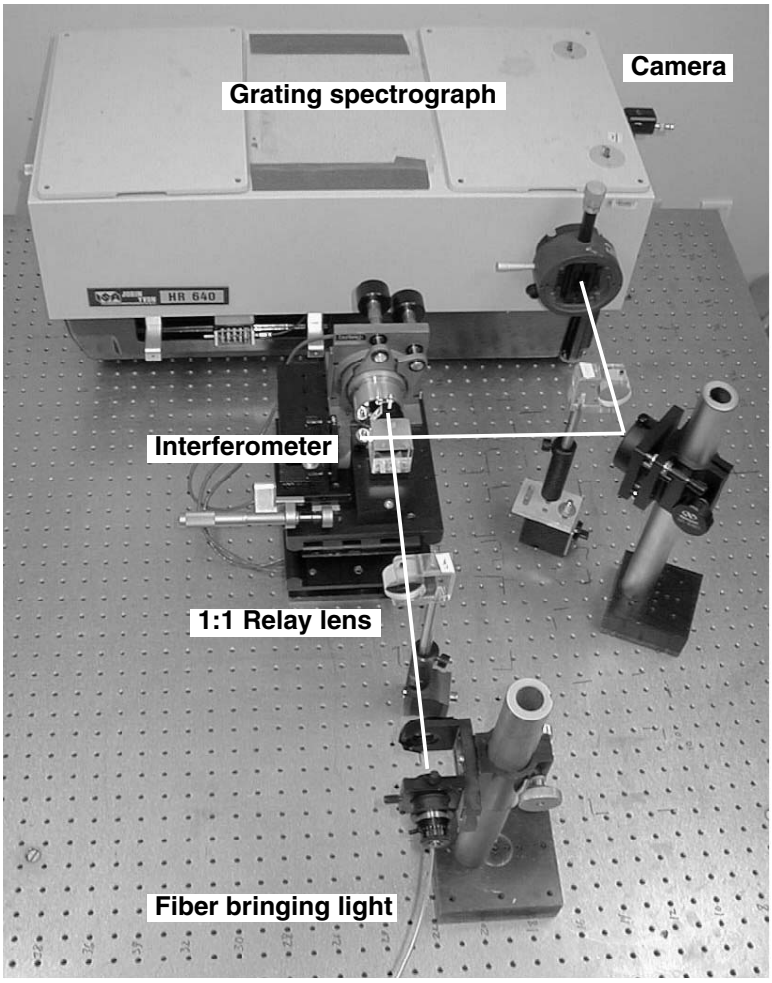

Figure 1. An EDI apparatus using a Jobin-Yvon linear grating spectrograph of ∼20,000 native resolution. The light source (fiber) is imaged to the angle-independent Michelson interferometer mirror plane, where fringes are created. This plane is then imaged to the slit plane of the spectrograph. Due to the nonzero interferometer delay, the fringes have sinusoidal wavelength dependence. This generates a comb of sinusoidal fiducials multiplying the input spectrum, over the entire bandwidth of spectrograph.

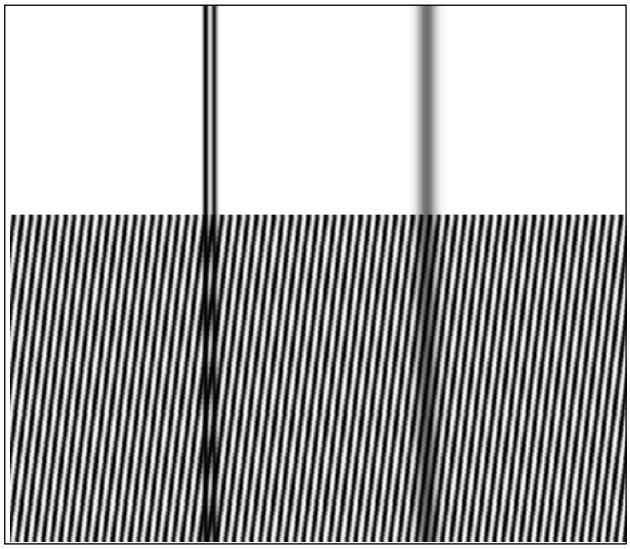

Figure 2. Graphical demonstration of the increased resolving power coming from a heterodyning effect. The classical definition of resolving power is the ability to distinguish a doublet from a singlet. If viewed from a distance, the doublet of lines on the left in the upper panel appears indistinguishable from the single line on the right. On the bottom panel a sinusoidal pattern is superimposed, representing the interferometer transmission. The presence of the generated moiré pattern immediately distinguishes the doublet. The amplitude and phase of the moiré pattern manifests the depth and position of the valley inside the doublet.

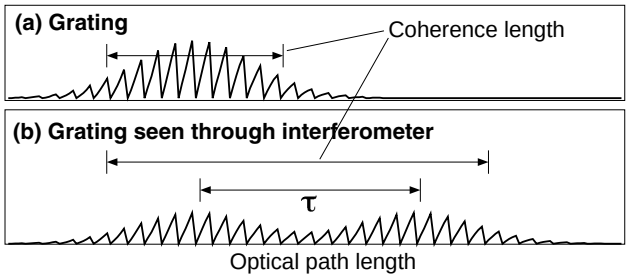

Figure 3. Apparent increase in coherence length of a grating when viewed through an interferometer having delay τ. The spectral resolution is proportional to the grating coherence length. Therefore the resolution of the net device increases.

1.1. Variety of applications

The EDI was originally developed for radial velocimetry. However the EDI's ability to measure precise ($\sim \lambda/20{,}000$) white light fringe shifts between simultaneous multiple spectral sources suggests additional metrology technologies. The EDI has been proposed (Erskine & Edelstein 2003a) to be used with a long baseline interferometer "front end" to measure precision angular differences between simultaneous multiple star targets. (Astrometry is another method of detecting exoplanets, through stellar displacement.) Because EDI spectral astrometry is a differential measurement, it is insensitive to microscopic drifts in the optical path length or interferometer baseline, a challenging problem for the conventional astrometry technique.

More recently, the EDI's has been applied to high resolution spectroscopy, either as a compact stand-alone instrument, or as performance boosting filter or insert to an existing spectrograph facility. This application is the focus of this article. Essentially, we have "eyeglasses" that can be inserted into the beam path of any spectrograph to boost its spectral resolution by factors of 2-10$\times$ or more.

The EDI can resolve features beyond the Nyquist limit of the CCD, because the moiré patterns encoding the high resolution information are broader than the CCD pixel spacing. Preliminary EDI data indicating an $\sim$8$\times$ resolution boost has been taken recently using multiple interferometer delays observing an iodine spectrum.

The EDI also improves spectrograph stability, because the broad moiré patterns are less susceptible to changes in shape of the light beam at the slit, aberrations of lenses in the spectrograph camera, and thermal or mechanical drifts of the CCD.

1.2. Sinusoidal fiducials

In comparison with other hybrids that use a Fabry-Perot interferometer to produce narrow impulse spectral fiducial fringes (McMillan et al. 1993), EDI's sinusoidal fiducial fringes transmit greater average flux, provide a heterodyning effect and Fourier interpretation, and allow elegant trigonometric recovery of precise spectral information from as few as three phase-stepped data recordings. The fiducials are easily removed by *summing* the phase stepped exposures, rather than by a division, avoiding divide-by-zero issues. This is not practical with non-sinusoidal fiducials. The ordinary spectrum is thus recovered along with new information contained in the fringing component. In this sense the fiducials are "transparent".

A Doppler shifted stellar spectrum causes the entire moiré pattern to phase shift, relative to a phase shift observed in a reference spectrum simultaneously observed, such as an iodine absorption cell. Hence for radial velocimetry the channel-by-channel moiré phase shift is averaged over all wavelength channels, i.e. its wavelength dependence is discarded.

In contrast, for the EDI spectroscopy application the wavelength dependence of the moiré pattern is analyzed. The heterodyning effect creating the moiré pattern optically is reversed numerically to recover high resolution information in the stellar spectrum. This is combined with lower resolution information of the ordinary spectrum, obtained from the same CCD data, to produce

a spectrum having effectively higher resolution than the grating spectrograph used without the interferometer.

1.3. Some Literature

Early EDI radial velocimetry work is described by Erskine & Ge (2000); Erskine (2002); Ge (2003). The first reference demonstrated 1 m/s scale precision in benchtop measurements on laboratory sources. The first EDI stellar radial velocimetry measurements, at the Lick Observatory 1 m in 1999, are described by Ge, Erskine, & Rushford (2002) and have few m/s precision. The EDI has been used to detect the exoplanet around 51 Pegasi at Kitt Peak (Ge et al. 2003).

Two different but related theories for EDI Doppler velocimetry exist, by Ge (2002) and by Erskine (2003). The latter provides a theoretical foundation for the heterodyning effect used in the resolution boosting application, and can be applied to echelle gratings and 1-D imaging spectrographs, as well as linear gratings. That is, the theory handles both uniform and transversely splayed phase along the spectrograph slit. Echelle gratings have tremendous bandwidth advantage over linear grating spectrographs and are used in the world's major observatories.

1.4. Resolution boosting for spectroscopy

The focus of this article is the use of the EDI to boost spectrograph resolution. This has been demonstrated for echelle and linear grating spectrographs in Erskine & Edelstein (2003b); Erskine et al. (2003).

Figure 2 is a graphical demonstration of resolution boosting. The classical definition of resolving power is the ability to distinguish between a doublet and singlet. In the top panel the two lines, viewed from a distance, appear similar. The bottom panel shows that after a sinusoidal grid is overlayed, it becomes obvious by the presence of the moiré fringes that the left line is a doublet, demonstrating that the resolving power has been increased. Furthermore the amplitude of the moiré yields the depth of the valley in between the doublet, and the phase of the moiré yields the detailed position of the doublet modulo the nearest fiducial fringe.

Coherence length increase An explanation of the resolution boosting effect is that the inclusion of the interferometer increases the apparent coherence length of a grating (Figure 3). The spectral resolution ($R \equiv \lambda/\Delta\lambda$) is limited by the grating coherence length, which is affected not only by the grating grooves but by the quality of the lenses internal to the spectrograph. An interferometer creates an echo delayed by time τ/c, where τ is the interferometer optical path length difference and c the speed of light. Thus any object viewed through the interferometer appears twice (with 50% amplitude for each image), but with the second image delayed in time. The two images of the grating, observed together, appear as a single grating with a longer coherence length, in spite of lesser quality lenses.

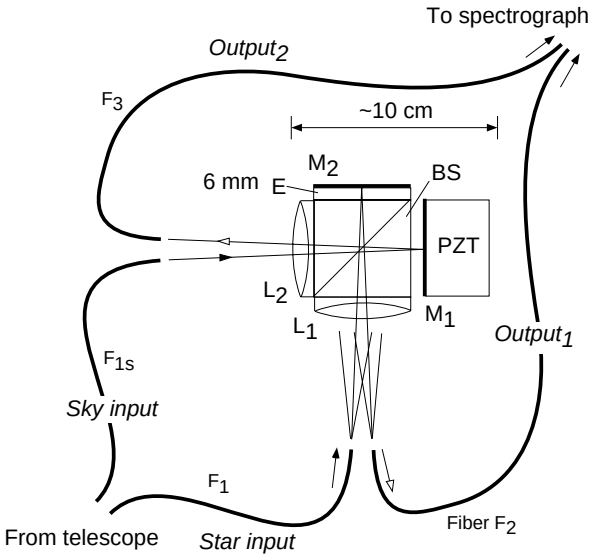

Figure 4. Scheme for a dual input, dual output EDI. Angle of incidence distinguishes inputs vs outputs. Sky fiber F_{1s} produces a fringing signal 180° out of phase with star fiber F_1 and therefore automatically subtracts without using extra CCD pixels. A 6 mm thick etalon (E) allows an angle-independent roundtrip delay of 11 mm, appropriate for boosting resolution of a R∼20,000 grating. Fibers F_2 and F_3 carrying complementary output signals would go to different positions along spectrograph entrance slit.

2. Theory

The goal of EDI spectroscopy data reduction is to start with the measured moiré fringes and work backwards to deduce the original spectrum.

2.1. Conventional spectroscopy

The conventional (purely dispersive spectroscopy) detected signal versus frequency, $B_{ord}(\nu)$, is the convolution of the intrinsic input spectrum, $S_0(\nu)$, and the spectrograph line spread function $LSF(\nu)$,

$$B_{ord}(\nu) = S_0(\nu) \otimes LSF(\nu) \tag{1}$$

where frequency is $\nu = 1/\lambda$ in units of cm^{-1}. The full width at half max (FWHM) of $LSF(\nu)$ is $\Delta\nu$ and is related to resolution by $R = \nu/\Delta\nu$. The convolution of Eq. 1 is conveniently expressed in Fourier-space,

$$b_{ord}(\rho) = s_0(\rho)\ lsf(\rho)\ , \tag{2}$$

where lower case symbols are the transformed versions, and ρ is the spatial frequency along the dispersion axis in cycles per cm^{-1}. The $lsf(\rho)$ is thus the transfer function of the impulse response $LSF(\nu)$.

2.2. EDI spectroscopy

Figure 4 (section 4.1) shows a scheme for directing both interferometer outputs to spectrograph slit. Hence, except for non-ideal interferometer mirror reflectivity and parasitic air/glass interface losses, all the flux entering the interferometer is utilized by the spectrograph. Then it is appropriate to use the normalized interferometer transmission $T'(\nu)$, which is a sinusoidal spectral comb

$$T'(\nu) = 1 + \gamma\cos(2\pi\tau\nu + \phi)\ , \tag{3}$$

where γ is the interferometer visibility, assumed unity for now, and τ is the interferometer delay in units of cm. Three or four spectra B_ϕ are recorded at phase values ϕ differing by 120° or 90°, respectively, and designated B_0, B_{90}, etc., so that the phases are distributed evenly around the circle.

The passage of light through the interferometer multiplies the spectral comb $T'(\nu)$ with the input spectrum *prior* to any blurring action from the external grating spectrograph. Hence the EDI detected signal is

$$B_\phi(\nu) = [S_0(\nu)\ T'(\nu)] \otimes LSF(\nu)\ . \tag{4}$$

Equation 4 is re-expressed as a sum of the ordinary spectrum plus two complex counter-rotating fringing terms

$$\begin{aligned} B_\phi(\nu) \quad = \quad & B_{ord}(\nu) + \tfrac{1}{2}[S_0(\nu)e^{i\phi}e^{i2\pi\tau\nu} + \\ & S_0(\nu)e^{-i\phi}e^{-i2\pi\tau\nu}] \otimes LSF(\nu). \end{aligned} \tag{5}$$

One needs to isolate a single fringing component. To do this, we form a linear combination of the phased exposures B_ϕ which have been numerically

rotated in synchrony with each exposure's phase-step value. This creates a complex *vector* spectrum called a "whirl", $\mathbf{W}(\nu)$, The linear combination cancels two out of the three components in Eq. 5. The general expression for a whirl for N-recordings (ϕ evenly spaced around the phase circle) is

$$\mathbf{W}(\nu) = \frac{1}{N} \sum B_\phi \; e^{i\phi} \tag{6}$$

and specifically for four phase recordings, every 90° is

$$\mathbf{W}(\nu) = \tfrac{1}{4}[(B_0 - B_{180}) + i(B_{90} - B_{270})] \; . \tag{7}$$

Applying Eq. 10 or 7 to Eq. 5 we get

$$\mathbf{W}(\nu) = \tfrac{1}{2}[e^{i2\pi\tau\nu} S_0(\nu)] \otimes LSF(\nu) \; . \tag{8}$$

The Fourier transform of the whirl is then

$$\mathbf{w}(\rho) = \tfrac{1}{2}\gamma \; s_0(\rho + \tau) \; lsf(\rho) \tag{9}$$

where we include the interferometer visibility (γ) previously taken as unity.

This important equation describes the EDI formation of moiré fringes, a heterodyning effect expressed in the $s_0(\rho + \tau)$ argument. Fine spectral details having high ρ are heterodyned (shifted by τ) to measurable low ρ prior to any blurring by the spectrograph's line spread function.

Obtaining the ordinary spectrum The ordinary spectrum is obtained from fringing spectra by summing several phase stepped exposures so that the fringing terms cancel,

$$B_{ord}(\nu) = \frac{1}{N} \sum B_\phi \tag{10}$$

or specifically for four recordings

$$B_{ord}(\nu) = \tfrac{1}{4}(B_0 + B_{180} + B_{90} + B_{270}) \; . \tag{11}$$

Hence an advantage of sinusoidal fringes is that they are transparent, in the sense that they can be easily removed to yield the ordinary spectrum. Both ordinary and fringing spectra are obtained from the same data set.

Heterodyning reversal The heterodyning is reversed by Fourier transforming the data from $\mathbf{W}(\nu)$ to $\mathbf{w}(\rho)$, translating it by τ, and then inverse Fourier transforming it back to ν-space. The procedure is described in more detail in Erskine et al. (2003).

Instrument response Figure 5 shows the transfer function of the conventional and EDI techniques, versus ρ. The higher the resolution, the broader is the response peak. The EDI response shows a new "treble" peak due to the heterodyning effect, displaced at $\rho = \tau$. By choosing τ to place this peak on the shoulder of the ordinary response ("bass"), the composite EDI response has a high-ρ behavior that approximately matches the conventional technique with a 2.4× higher resolution.

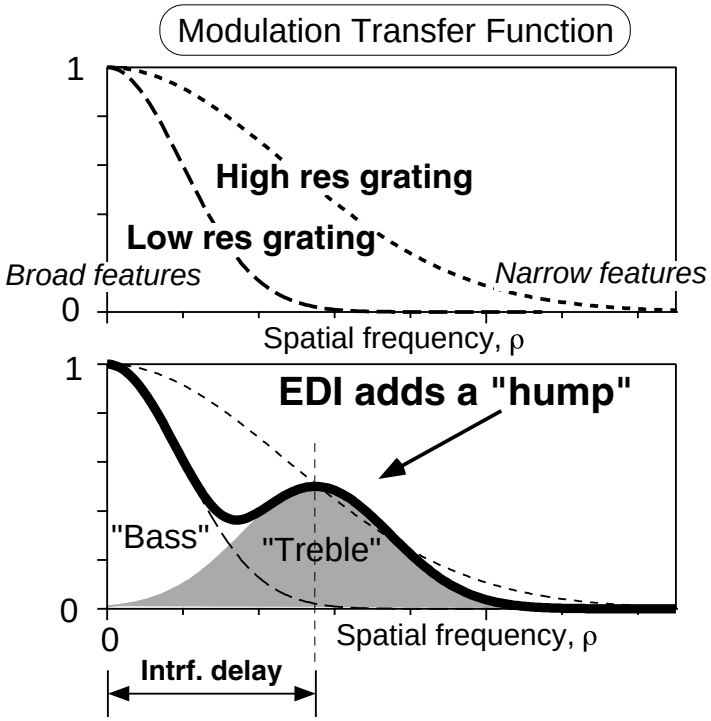

Figure 5. Conventional and EDI instrument transfer functions, i.e. the ability to detect a given spatial frequency (ρ) along the dispersion axis. High spectral resolution requires a broad modulation transfer function. (a) low and high resolution gratings, 2.4× different, are plotted as long and short dashed curves. (b) The interferometer creates a hump in the response that is the same shape as the intrinsic response (long dashes) but displaced by the interferometer delay, and half as high. For a particular delay the EDI high spatial frequency behavior is similar to that of a $\sim 2.4\times$ greater resolution grating (short dashed curve). All curves have been normalized to the same photon noise. Units of ρ are cycles per cm^{-1}, or cm.

Equalization removes notch The notch in the net EDI response between the bass and treble peaks can be removed by changing the weighting of the ρ-components in an equalization step. This moderately increases the continuum noise for mid level ρ, but not for low or high ρ. Since science features typically reside in the highest ρ of a spectrum, the EDI boost is useful.

Figure 6 numerically simulates the detection of an absorption line doublet by conventional and EDI methods, including equalization, using the same raw CCD "data" containing added random noise simulating photon statistics. The 2.4× boosting effect is confirmed. This also shows that the minor increase in noise for mid-ρ's during equalization does not prevent resolving the doublet, for the 1.24% level of continuum random noise used.

3. Example Data

The EDI can be used with the phase of the interferometer comb being either constant or linearly splayed over the beam area. The former allows use with echelle spectrographs and 1-d imaging spectrographs using at least three phase stepped exposures, and the latter allows use with a linear grating obtaining all the needed phase information in a single exposure. Figure 7 shows a section of EDI fringing spectra from the Lick Observatory echelle spectrograph observing ϵ-Leo. Several orders, including the Na doublet, are shown. The bead-like structure in the continuum areas are the sinusoidal fiducials. Figure 8 shows the effect of stepping the interferometer phase observing a single order containing the telluric lines. The change in appearance with phase indicates that the spectrum has structure at the periodicity of the interferometer, which is $\sim$0.9 cm^{-1} for that Figure. Figure 9 demonstrates a $\sim$2× resolution boosting effect on the echelle (50,000 $\rightarrow$ 100,000) using a 3 cm delay interferometer, comparing conventional and EDI spectra in the telluric region of α-Virgo.

4. On-going work: Multiple delay EDI

Figure 10 shows the theoretical response of an EDI using M multiple interferometer delays. Data could be taken sequentially or in parallel. Each delay produces a heterodyning peak translated to a different ρ-value so that the concatenate response is extended to $(2M + 1)$ higher ρ than the grating used alone. Hence, after equalization to remove the bumps in the response, the effective resolution can be $(2M + 1)$ times the intrinsic grating resolution. The height of the heterodyned response peaks have been reduced by $\sqrt{M}$ from the ideal single delay value (0.5) to reflect the partition of the same number of photons into M times more exposures.

Experimental work is underway to demonstrate 10× resolution boosting using multiple delays on the linear grating EDI pictured in Fig. 1. Preliminary fringing spectra taken October 2003 of the iodine spectrum using a series of delays detects features up to $\sim$170,000 resolution, $\sim 8\times$ finer than the $\sim$20,000 intrinsic resolution of the Jobin-Yvon spectrograph.

In the limit where many discrete delay steps become a continuous scan, multiple delay EDI spectroscopy is related to Fourier Transform spectroscopy

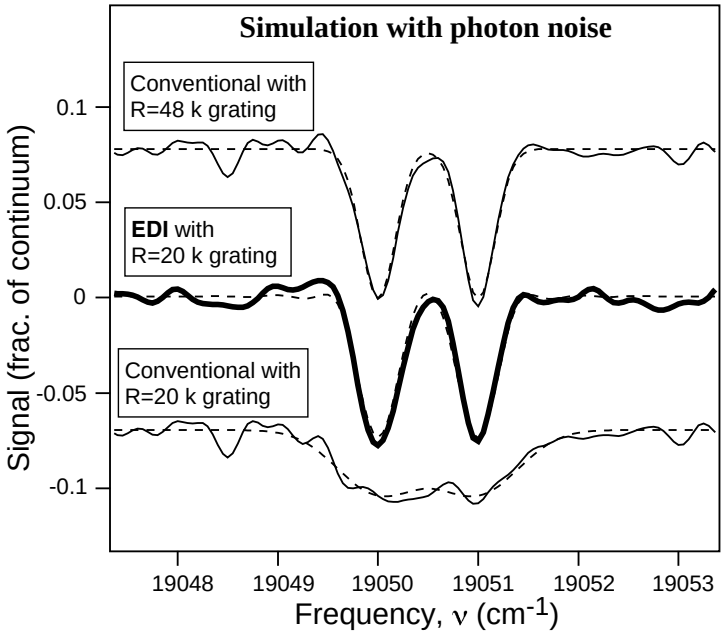

Figure 6. Numerical simulation comparing conventional and EDI techniques in resolving an absorption line doublet under the effect of photon noise. Bold curves include simulated photon noise 1.24% of continuum at pixel size 6 per cm^{-1}. The same noise field is added to the raw "CCD" data for each case, (heterodyning causes the EDI noise to appear differently). Dashed curves are noiseless. The subject is a pair of Gaussian absorption lines of 50% depth, 0.0625 cm^{-1} width and separated by 1 cm^{-1}. A 2.4 times resolution boosting effect is demonstrated. Equalization was used to bring the effective EDI lineshape to a Gaussian shape. This has the side effect of enhancing continuum noise near $\sim$1.6 cm^{-1} spatial period, but the simulation shows the resulting total noise is similar to the conventional method at higher resolution, regarding its ability to resolve the doublet.

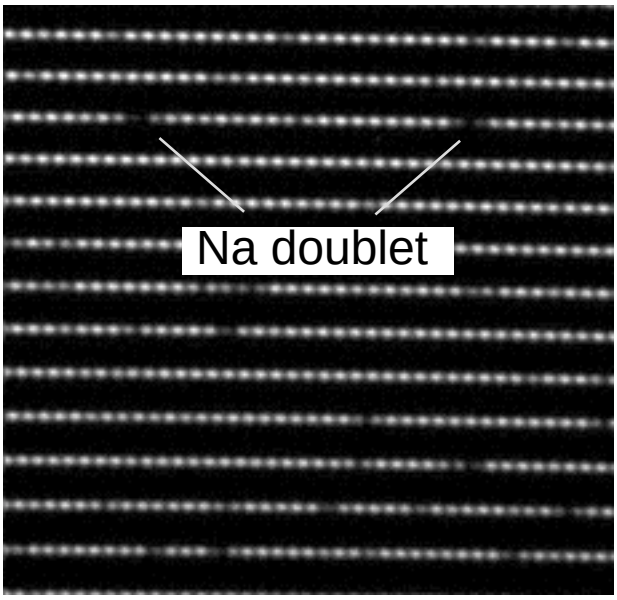

Figure 7. Example EDI echelle CCD data of ϵ-Leo, showing several orders including the sodium doublet. Only a small subset of the full CCD chip is shown. Note the periodic "bead-like" fiducials which overlay the stellar spectrum, which is the result of the interferometer. Their spacing is 0.9 cm^{-1}.

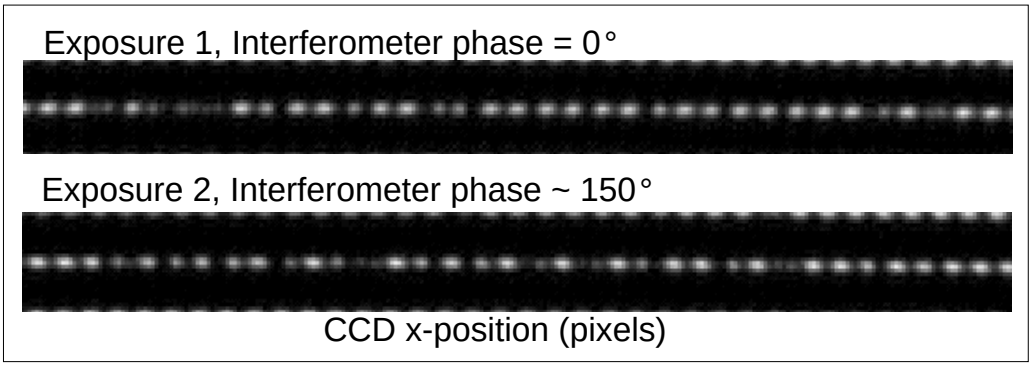

Figure 8. The effect of changing the interferometer phase on a stellar fringing spectrum. Two exposures of the telluric feature near 6868 Å of ϵ-Leo are shown. When the interferometer phase changes 150° between them, the moiré pattern also changes, indicating stellar features similar to the fiducial spacing are present. At least three exposures spaced ∼120°, or four spaced ∼90°, are needed to arithmetically separate the fringing component (moiré) from the underlying ordinary spectrum.

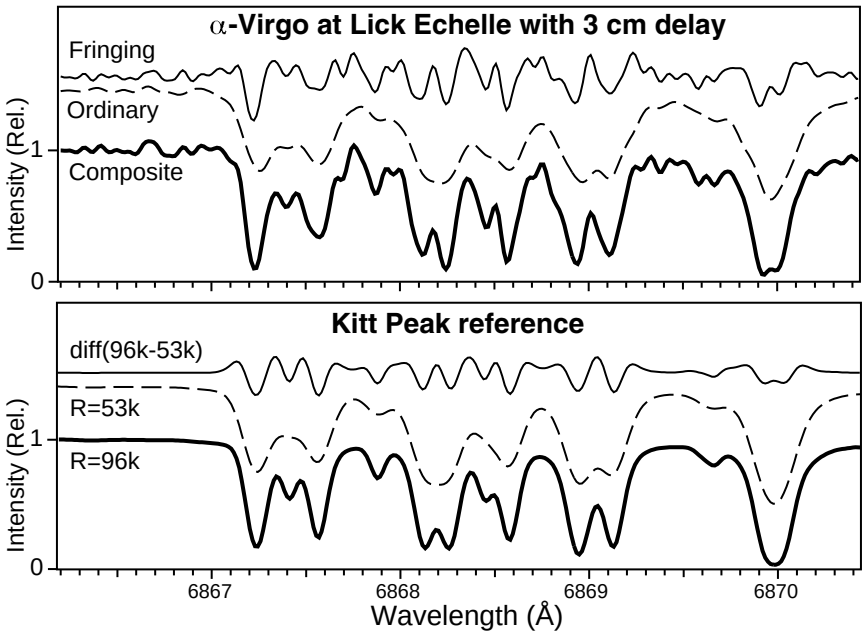

Figure 9. EDI spectral resolution boosting of $\sim 2\times$ is demonstrated for oxygen telluric lines in the Lick R=50,000 echelle spectrum of α–Virgo. Top: The measured EDI ordinary spectrum (dashed line) and fringing spectrum using a 3 cm delay (thin line) are combined to form the composite spectrum (bold line). The fringing spectrum provides high-frequency information that boosts effective resolution. Bottom: Reference solar spectrum blurred to R=53,000 (dashed line), 96,000 (bold line), and their difference (thin line) compare closely to the EDI spectral components and composite. The curves are vertically offset. Data at the ends of the band were truncated in analyses.

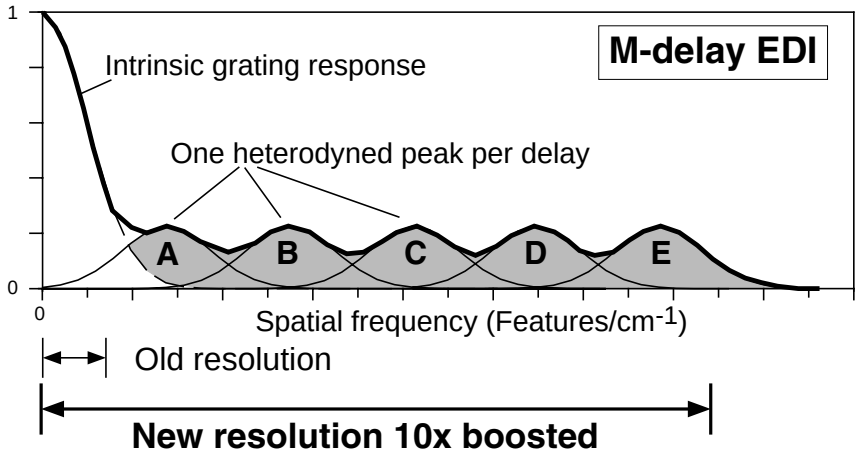

Figure 10. A method of achieving arbitrarily higher spectral resolution is to take a series of exposures at M-different delay values, and concatenate the results. The resolution boosting factor will be $\sim$(2 M + 1). To normalize to the same photon noise, the height of each heterodyned peak has been reduced by $\sqrt{M}$ from its single delay value. The net instrumental noise will be greatly reduced over the case of a ordinary spectrograph with its slit width smaller by (2M + 1), since instrumental noise is minimal at the center of each heterodyned peak. This concept of discretely changing the delay is related to Fourier transform spectrographs where the delay is continuously changed, but the EDI can have 2 orders of magnitude better photon signal to noise ratio since it uses all the spatial frequencies in the CCD instead of only the DC component.

(FTS), but has 100× better photon signal to noise ratio over the optical bandwidth. This is due to EDI's use of all the spatial frequencies on the CCD rather than just the DC (constant) component.

4.1. Full-pass interferometer designs

To pass all the photons, both complementary interferometer outputs need to be used. Several interferometer designs for providing dual outputs have been identified, some working with open beams and others with fibers. The outputs are directed to slightly different places on the spectrograph slit (otherwise the fringes would cancel). Figure 4 is one example. Schemes for interdigitating the 0° and 180° outputs into the space between echelle orders have been developed. Note, by recording the 0° and 180° data simultaneously, only two separate exposures are needed to provide a full circle of phase steps.

Borrowing an idea from FTS instruments, a complementary output interferometer can also provide complementary inputs, one of which can be assigned to the "sky" so that its fringing output optically subtracts from the primary input. This is a means of automatically subtracting a sky background. (The ordinary spectrum does not have this feature, so this advantage is particularly strong for a multiple-delay EDI where the majority of the signal is fringing. Edelstein (2003) has pointed out that this capability can be used to measure differential velocity fields or differential lineshapes in extended objects.

Acknowledgments. My collaborators Jerry Edelstein, Barry Welsh and Michael Feuerstein of the Space Sciences Lab., Univ. of California, Berkeley assisted in taking the Lick echelle data. Thanks to the Lick Observatory and staff for their facility. Reference iodine spectra were provided by Kitt Peak/NOAO. Work was supported by CalSpace/Lockheed, NASA grants NAG5-9091 and NAG5-3051. This work was performed under the auspices of the U.S. Department of Energy by the University of California, Lawrence Livermore National Laboratory under contract No. W-7405-Eng-48.

References

Douglas, N. 1997, PASP, 109, 151

Edelstein, J. 2003, personal communication

Erskine, D. J. 2002, Combined Dispersive/Interference Spectroscopy for Producing a Vector Spectrum, US Patent Number 6,351,307, issued 26 February 2002

Erskine, D. J. 2003, PASP, 115, 255

Erskine, D. J., & Edelstein, J. 2003a, in SPIE Conf. Proc., 4852, Spectral astrometry mission for planets detection, ed. Michael Shao, 695

Erskine, D. J., & Edelstein, J. 2003b, in SPIE Conf. Proc., 4854, Future EUV/UV and Visible Space Astrophysics Missions and Instrumentation, ed. J. C. Blades, O. H. Siegmund, 158

Erskine, D. J., Edelstein, J., Feuerstein, W. M. & Welsh, B. 2003, ApJ, 592, L103–L106

Erskine, D. J., & Ge, J. 2000, in ASP Conf. 195, Imaging the Universe in Three Dimensions: Astrophysics with Advanced Multi-Wavelength Imaging Devices, ed. W. van Breugel & J. Bland-Hawthorn, 501

Ge, J. 2002, ApJ, 571, L165

Ge, J. 2003, ApJ, 593, L147

Ge, J., Erskine, D. J., & Rushford, M. 2002, PASP, 114, 1016

Ge, J., van Eyken, J., DeWitt, C., & Shaklan, S. 2003, NOAO-NSO Newsletter, March, 73, 31

Harlander, J., Reynolds, R., & Roesler, F. 1992, ApJ, 396, 730

Hilliard, J., & Shepherd, G. 1966, J. Opt. Soc. Am., 56, 362

McMillan, R. S., Moore, T. L., Perry, M. L., & Smith, P. H. 1993, ApJ, 403, 801